ELSEVIER

Contents lists available at ScienceDirect

Microporous and Mesoporous Materials

journal homepage: http://www.elsevier.com/locate/micromeso



Calculated infrared and Raman signatures of Ag^+ , Cd^{2+} , Pb^{2+} , Hg^{2+} , Ca^{2+} , Mg^{2+} , and K^+ sodalites



Amir Mehdi Mofrad ^a, Parker S. Schellenberg ^{a,1}, Caio Peixoto ^a, Heather K. Hunt ^a, Karl D. Hammond ^{a,b,*}

- ^a Department of Biomedical, Biological, and Chemical Engineering, University of Missouri, Columbia, MO, 65211, USA
- ^b Nuclear Engineering Program, University of Missouri, Columbia, MO, 65211, USA

ARTICLE INFO

Keywords: Sodalite DFT Vibrational spectroscopy Ion exchange Heavy metals

ABSTRACT

We explore the potential of vibrational spectroscopy, an inexpensive analysis technique, for the purpose of detecting of heavy metals in water using sodalite. Computations via density functional theory of the infrared and Raman spectra of anion-free sodalites that have been exchanged with lead (II), cadmium (II), and mercury (II) ions predict a peak in the 850–880 cm⁻¹ range in both the infrared and Raman spectra that is characteristic of anion-free sodalites that have been exchanged with these three heavy metal cations. This peak is distinguishable from the infrared spectra of anion-free sodalites that have been exchanged with potassium, magnesium, and calcium ions, which are naturally present in drinking water. Unfortunately, no peak in this range exists for chloro-, bromo-, or hydroxy-sodalites, and peaks in this range may be masked by the presence of magnesium hydroxysodalites, which would be expected to form in water testing applications. In addition, the signal-to-noise ratio is likely too low to provide a useful test for heavy metal contamination at the levels required for municipal water testing.

1. Introduction

The release of heavy metals into soil and water is a worldwide environmental concern [1]. Heavy metals tend to accumulate in the soil and in living organisms, causing health problems that affect the kidneys, the central nervous system, blood cell production (hematopoiesis), and the gastrointestinal tract [2]. The World Health Organization (WHO) recommends extremely low thresholds for acceptable levels of heavy metal cations in drinking water (2–15 ppb, depending on the metal type) [3–5]. Consequently, many efforts have been made to improve existing methods for removal of such contaminants. Electrochemical treatment, adsorption, reverse osmosis, and ion exchange have all been utilized to capture heavy metal ions from water [6-9]. Chemical and electrochemical treatments, as well as reverse osmosis methods, have been shown to reduce the concentrations of heavy metals significantly, but only when ion concentrations are high (i.e., above 500 mg/L) [10,11]. The major drawback of using these methods, particularly reverse osmosis, is their immense power consumption for pumping, as well as the expense involved in producing the membranes [12]. Conversely, ion

exchange by zeolites has been shown to be more efficient at removing heavy metal ions from water at all concentrations, both in terms of cost and ion removal capacity [4,12].

Zeolites are porous aluminosilicate materials used for a variety of industrial processes, such as gas separation, ion exchange, and catalysis [13,14]. In zeolites with a one-to-one ratio of silicon to aluminum (Si/Al = 1), alternating SiO₄ and AlO₄ tetrahedra (according to Löwenstein's rule [15]) are linked together in a way that creates a three-dimensional network with channels and/or pores of uniform sizes. There are, to date, 248 unique zeolite framework topologies that occur naturally and/or synthetically [16]. Sodalite (framework code SOD), whose structure was determined about 80 years earlier than any other zeolite [17], is one of the simplest and most symmetrical frameworks. Because of its cage-like structure, it can host a regular array of well-defined nanoclusters, which would result in the creation of sodalite-based materials with potentially useful catalytic, magnetic, optical, vibrational, and electronic properties [18,19]. For instance, optical applications of sodalite date from the 1970s, when photochromic and cathodochromic sodalites were used for information storage and filter optics [20,21]. Sodalite has also been

^{*} Corresponding author. Department of Biomedical, Biological, and Chemical Engineering, University of Missouri, Columbia, MO, 65211, USA. *E-mail address:* hammondkd@missouri.edu (K.D. Hammond).

 $^{^{1}\,}$ Current affiliation: Core and Main, Rochester, New York (USA).

modified to function as a catalyst in base-catalyzed reactions [22]. In all applications of sodalite—as with zeolites in general—synthesis and characterization techniques are important to ensure the materials have consistent and known physical and chemical properties.

Spectroscopic techniques, particularly infrared and Raman, are often used in the characterization of zeolites [23]. These techniques can identify characteristic vibrations associated with secondary building blocks (SBU), extra-framework cations, and lattice vibrations [24–27]. In particular, we anticipate there will be a measurable difference in the IR or Raman spectrum of sodalite that has been exposed to heavy metal cations compared with the natural (sodium) form. Unfortunately, due to the structural complexity of zeolites, interpretation of experimental vibrational spectra is often troublesome and relies heavily on supposition [28]. Computational tools are therefore helpful in obtaining more accurate insight into the spectroscopic properties of zeolites.

Computational vibrational spectroscopy based on density functional theory (DFT) can be helpful in interpreting zeolite vibrational spectra [23,29–31]. Furthermore, thanks to advancements in computing, the prediction of vibrational frequencies in zeolites has become feasible. Due to the presence of finite-size effects, employing periodic boundary condition (PBC) calculations provides better agreement between experiments and simulations than non-periodic cluster calculations [32].

In this study, we investigate the sensitivity of computational vibrational spectroscopy for the purpose of detecting ion exchange levels in sodalite. We hypothesize that infrared and/or Raman spectra of either partially or completely ion-exchanged anhydrous sodalite are capable of detecting the presence of contaminants such as Cd^{2+} , Pb^{2+} , and Hg^{2+} in the presence of other cations that are normally present in water, such as sodium, potassium, magnesium, and calcium.

We start by comparing the measured and calculated infrared spectra of sodium chlorosodalite—that is, $|Na_8Cl_2|$ $[Si_6Al_6O_{24}]\text{-}\mathbf{SOD}$, which is the composition of naturally-occurring sodalite—and the equivalent bromide form, $|Na_8Br_2|$ $[Si_6Al_6O_{24}]\text{-}\mathbf{SOD}$, as well as the infrared spectra of chlorosodalites exchanged with silver, cadmium, and lead ions. We then examine the computed infrared and Raman spectra of anion-free sodalite, $|Na_6|$ $[Si_6Al_6O_{24}]\text{-}\mathbf{SOD}$, and hydroxysodalite, $|Na_8(OH)_2|$ $[Si_6Al_6O_{24}]\text{-}\mathbf{SOD}$, as well as the same materials exchanged with heavy metal cations. We also consider the effects of exchange with ions normally present in water, including potassium, magnesium, and calcium ions.

The chloro- and bromo-sodalites do not show a distinct "signature" of heavy metal exchange, nor do the hydroxy-sodalites. However, the anion-free sodalites show a characteristic additional peak in the 850–880 cm⁻¹, which appears to be diagnostic of the presence of lead, cadmium, and/or mercury. Unfortunately, this peak is not expected to be particularly prominent in the experimental spectrum, and its presence may also be masked by the presence of magnesium ions: magnesium ions show a similar peak for hydroxy-sodalites, though not in anion-free sodalites. While the Raman spectrum could, in principle, be able to distinguish between these two scenarios, the practicalities of infrared and Raman spectroscopy combined with the relatively weak intensity of these peaks strongly suggest that vibrational spectroscopy will not be a viable method of detecting lead or other heavy metals in zeolites at relevant concentrations.

2. Notation and methodology

2.1. Simplified notation

Natural sodalite is predominantly $|Na_8Cl_2|$ [Si₆Al₆O₂₄]-**SOD**. Due to numerous possible variations that can occur when synthesizing sodalite, a variety of compositions can result that follow the general formula [33]

$$|\mathbf{M}_{m}^{q+}\mathbf{X}_{x}^{r-}|[\mathbf{Si}_{12-n}\mathbf{Al}_{n}\mathbf{O}_{24}(\mathbf{H}_{2}\mathbf{O})_{0-8}] - \mathbf{SOD},$$
 (1)

where qm - rx = n and $n \le 6$. Fig. 1 shows a bromosodalite partially

exchanged with lead (II) ions (it should be noted, as we will discuss later, that this structure does not exhibit a definitive "signature" in the vibrational spectra). In Equation (1), silicon and aluminum are the framework atoms; because they form tetrahedra with bridging oxygens, they are called T-atoms. The aluminum atoms that impart negative charges to the framework are compensated for by extra-framework sodium. Due to the presence of two bromide ions (or other anions), there need to be two more sodium cations per formula unit than required by the framework charge itself to neutralize the whole crystal. Therefore, in a sodalite unit cell, there are eight sites available for monovalent cations and two sites available for monovalent anions. Additionally, as shown in Fig. 1, the SBUs in the SOD framework are six single-four-membered rings (S4R) and eight single-six-membered-rings (S6R) per sodalite cage (the truncated octahedron in Fig. 1). The cationic positions are located at the center of the S6Rs, behind or in front of the plane of the ring. The standard notation [34] for sodalites with Si/Al = 1, the only Si/Al ratio studied herein, would always contain the group [Si₆Al₆O₂₄]; we instead adopt the following shortened notation for convenience:

$$|C_c A_a| - \mathbf{SOD} \Leftrightarrow |C_c A_a| [\operatorname{Si}_6 \operatorname{Al}_6 O_{24}] - \mathbf{SOD},$$
 (2)

where C refers to the cation and A refers to the anion. In the case of partial cation exchange, two cation symbols are used. For example, | Na_8Br_2 |-SOD refers to | Na_8Br_2 | [Si₆Al₆O₂₄]-SOD, |Ca₃|-SOD refers to anion-free |Ca₃| [Si₆Al₆O₂₄]-SOD, and | Na_4Pb |-SOD refers to partially-lead-exchanged, anion-free sodalite, | Na_4Pb | [Si₆Al₆O₂₄]-SOD. If there are no aluminum framework atoms present in the unit cell, it is referred to as siliceous sodalite, [Si₁₂O₂₄]-SOD, which is the simplest and most symmetrical of all zeolitic materials.

In the case of divalent cations (e.g., Ca^{2+}), it is necessary to iterate over all possible combinations of cation sites to find the minimum-energy configuration. From the point of view of theory, choosing anhydrous sodalite ($|\text{Na}_6|$ -SOD) over anion-bearing sodalite ($|\text{Na}_8\text{Cl}_2|$ -SOD) has two advantages: (i) the number of simulations to span all unique periodic unit cells is smaller in the anhydrous sodalite case than in the anion-bearing case; (ii) the cell volume of anhydrous sodalite is larger, which in principle means it might incorporate guest species more

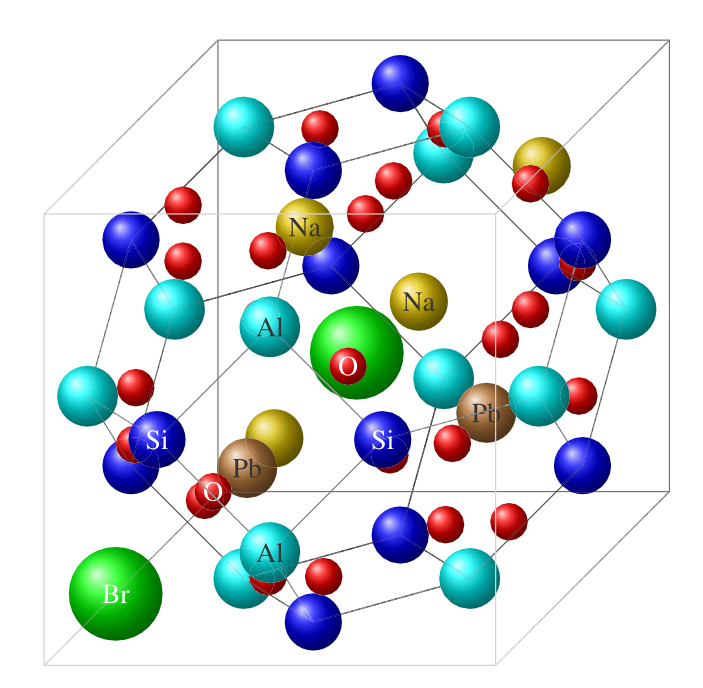


Fig. 1. The structure of a partially-lead-exchanged sodalite (**SOD** framework). Spheres are color-coded and drawn with a radius half the value of either the ionic radius (Br⁻, Na⁺, Pb²⁺) or the covalent radius (Al, Si, O). Sodalite has a simpler structure, higher degree of symmetry, and smaller number of atoms per unit cell than most other zeolites.

easily.

2.2. Electronic structure calculations

The crystal structure was generated with the $P\overline{4}3n$ space group (no. 218) as Felsche et al. [35] and Hassan et al. [36] suggested. The parent compound was the sodium form, $|Na_6|$ -SOD, and we based our analyses of the ion-exchanged materials on this parent crystal.

Electronic structure calculations were performed within the DFT formalism [37,38] using norm-conserving pseudopotentials [39,40] and the local density approximation (LDA) [38,41–44] as implemented in QuantumEspresso [45]. The reason why we chose norm-conserving LDA was primarily because the current version of QuantumEspresso computes Raman frequencies only at this level of theory. Moreover, our previous work [29] showed that this set of pseudopotentials with the LDA gives reasonable IR and Raman results that agree fairly well with experiment. We found that energies were converged with respect to basis set using a plane-wave cutoff energy of 80 Ry. The Brillouin zone was sampled using a Monkhorst–Pack [46] grid; we found that a $2 \times 2 \times 2$ grid produced a high enough k-point density for the results to be considered converged.

After the convergence test, we did a variable-volume geometry optimization in which both the ions' positions and the cell parameters were optimized simultaneously. The convergence threshold on the forces per atom was set to 10⁻⁷ Ry/Bohr. The optimization used the Brovden-Fletcher-Goldfarb-Shanno (BFGS) algorithm [47], a quasi-Newton method. The self-consistent field (SCF) calculations used a stopping criterion of 10⁻⁸ Ry. After geometry optimization, we performed phonon calculations based on density functional perturbation theory (DFPT) [45] at the center of the Brillouin zone (Γ point) to generate the dynamical matrix, from which vibrational frequencies were generated based on the acoustic sum rule [48]. The computed Raman activities were based on Placzek's theory of polarizability [49]; the self-consistency tolerance in the phonon calculations (tr2_ph) was set to 10⁻¹⁴ Ry. Both infrared and Raman spectra were line-broadened using Gaussian functions with full widths at half maxima of 20 cm⁻¹ (FWHM = 20 cm^{-1}); the heights were proportional to the intensities calculated for the corresponding normal modes of vibration.

2.3. Experiments

In an effort to check our results, we synthesized and/or ion-exchanged many of the materials mentioned in the remainder of this study. These materials were characterized by X-ray diffraction (XRD), energy-dispersive X-ray (EDX) analysis, and Fourier transform infrared

spectroscopy (FTIR). Information regarding synthesis and handling procedures, instrumentation, chemicals, and characterization is discussed thoroughly in the Supplementary Data. Many of the ion exchange procedures, in particular, were unsuccessful, so we instead compare our results primarily to previously-published experiments.

3. Results and discussion

3.1. Structural properties of anhydrous and anion-bearing sodalites

Table 1 shows the calculated structural properties of sodalite exchanged with different cations and anions. In the case of anion-containing sodalites, the cell volume is a function of both cationic radius as well as anionic radius and each atom's electronegativity. For example, according to Shannon [50], the K^{+} ionic radius is 138 pm, larger than any other cation in Table 1. However, the cell volumes of $\mid Pb_4Cl_2 \mid$ -SOD and $\mid Pb_4Br_2 \mid$ -SOD are slightly larger than those of their potassium counterparts, even though there are fewer cations present in the lead cases and the Pb^{2+} ion is smaller than the K^{+} ion. The reason for this is that the electronegativity of lead is significantly higher than potassium, which makes these cations less bound to the framework, resulting in a larger unit cell. Conversely, sodalites with bromide as the extra-framework anion have larger unit cells compared to chloride sodalites, as one would expect, because of the difference in ionic radius between the two anions.

For the anhydrous sodalites in Table 1, the cell volume of each material is larger than that of its anion-bearing counterparts, even though there are fewer cations and anions in the structure in the anion-free case. This again stems from the fact that the Coulombic forces between anions and cations draw the extra-framework cations closer to the anions and framework aluminum, causing the structure to shrink [51].

Finally, some of the compositions in Table 1 yield a slight distortion from cubic symmetry. This is primarily because of the arrangement of cations when they partially occupy the structure (i.e., extraframework cation vacancies are present). This deviation from cubic symmetry at an energetic minimum is expected: Latturner et al. [52] reported a phase transition temperature of 250 °C between the non-cubic and cubic variants of anion-free sodalite, with the low-temperature structure being associated with ordered Na_3^{3+} triangles. At high temperatures, thermal vibrations are larger than the energy gained by forming these structures, and cubic symmetry is restored.

3.2. Comparison with experiments

This section compares theoretical infrared spectra with both our own

Table 1

The structural properties of sodalite unit cells with different compositions. As anions are introduced into the structure, their negative charge attracts the cations, leading to shrinkage of the unit cell. Counterintuitively, the cell size does not depend significantly on the number of ionic species.

Compound	Volume (ų)	a (Å)	b (Å)	c (Å)	α (°)	β (°)	γ (°)
Na ₆ -SOD	711.079 (713.188) ^a	8.926 (8.935)	8.926	8.926	89.44	90.56	89.44
K ₆ -SOD	765.542 (768.230)	9.148 (9.159)	9.148	9.148	90.07	90.07	90.07
Cd ₃ -SOD	717.958 (720.719)	8.954 (8.966)	8.955	8.955	90.68	90.68	89.32
Pb ₃ -SOD	693.677 (693.438)	8.852 (8.851)	8.852	8.852	90.50	90.50	89.50
Na ₈ Cl ₂ -SOD	658.030	8.698	8.698	8.698	90	90	90
K ₈ Cl ₂ -SOD	731.213	9.009	9.009	9.009	90	90	90
Ag ₈ Cl ₂ -SOD	667.487	8.739	8.739	8.739	90	90	90
Cd ₄ Cl ₂ -SOD	663.632	8.646	8.878	8.646	89.99	90.27	89.99
Pb ₄ Cl ₂ -SOD	734.823	9.026	9.023	9.026	90.17	88.47	89.83
Na ₈ Br ₂ -SOD	671.301	8.756	8.756	8.756	90	90	90
$ K_8Br_2 $ -SOD	741.527	9.051	9.051	9.051	90	90	90
Ag ₈ Br ₂ -SOD	677.763	8.784	8.784	8.784	90	90	90
Cd ₄ Br ₂ - SOD	663.190	8.663	8.663	8.836	90	90	90
Pb ₄ Br ₂ -SOD	749.627	9.084	9.084	9.084	89.73	89.73	89.73

^a Numbers in parentheses correspond to the same starting configuration, except that it has been forced to have cubic symmetry ($\alpha = \beta = \gamma = 90^{\circ}$ and a = b = c). The experimental crystallographic parameters would be averages of configurations with vacancies at different sites, meaning the measured lattice parameters of any material with vacant extraframework cation sites would likely be intermediate between the two values even if the model were 100% accurate.

experimental results and findings from Mikuła et al. [53]. Fig. S1 in the Supplementary Data shows the measured XRD patterns of the parent compound and the ion-exchanged sodalites, as well as potassium chlorosodalite. Lead-exchange of sodium bromosodalite decomposed the crystal structure, and replacing sodium with potassium in the established protocol for sodium chlorosodalite [21] did not yield a sodalite phase; this is evident in the materials' XRD patterns. The infrared spectra of the compounds that yielded sodalite phases are not in good agreement with the IR spectra predicted by DFT (see Fig. S4, Supplementary Data) due primarily to unsuccessful ion exchange of those cations with the parent compound (see Table S1, Supplementary Data). It should be noted that the resulting sodalites are still sodium bromosodalites ($|Na_8Br_2|$ -SOD); consequently, any evidence of Pb^{2+} , Ag^+ , or Li^+ would be absent.

There are several reasons why these ion exchange protocols were unsuccessful. The potassium chlorosodalite synthesis was a modification of an established protocol for the sodium form; it appears that equimolar replacement of sodium with potassium during synthesis is inadvisable (see Fig. S1f, Supplementary Data). The failed lead exchange may have been a result of pH: zeolites are synthesized in strongly basic solution (i. e., pH> 11) [54], but the lead nitrate solution in our experiments had a pH of approximately 4, which may have been low enough to damage the structure (see Fig. S1e, Supplementary Data). For the other ion exchanges attempted (Li⁺, Ag⁺, and K⁺), the XRD patterns indicate the resulting materials are sodalites, but EDX indicated that very little ion exchange occurred. The lithium and potassium exchange protocols were originally tested on hydroxysodalites, not bromosodalites; their failure in the bromosodalite case may indicate that the anion makes a

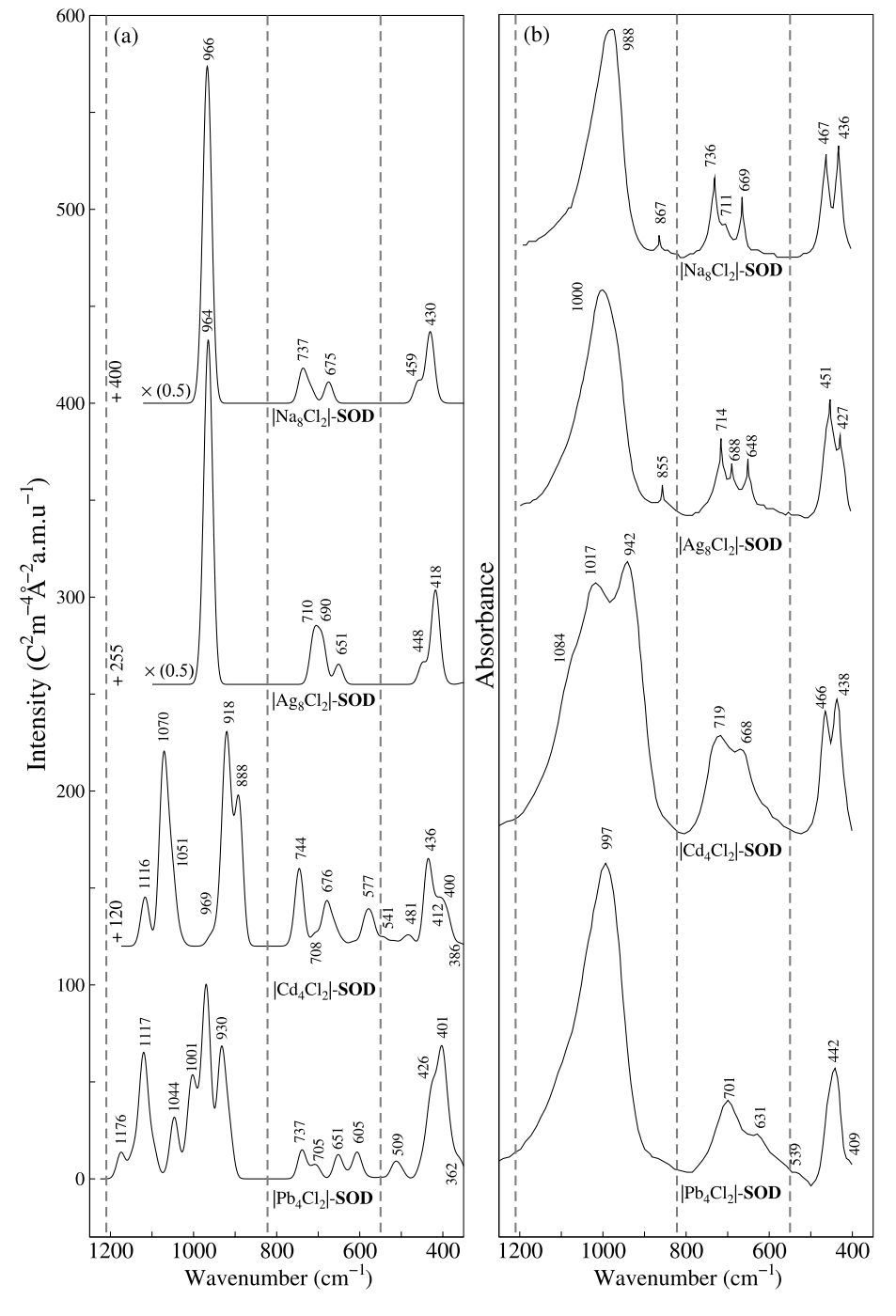


Fig. 2. (a) Calculated and (b) measured mid-infrared spectra of chlorine-bearing sodalite exchanged with Ag^+ , Cd^{2+} , and Pb^{2+} . The three regions separated by dashed lines correspond to asymmetric stretching, symmetric stretching, and bending modes from left to right. The corresponding vibrational wavenumbers are written above each peak. The intensity in the computed spectrum is proportional to absorbance. Graphs are translated and scaled by the values written next to them. Experimental data are from Mikula et al.

significant difference to the mechanism and/or rate of ion exchange. The silver exchange protocol was also developed for hydroxysodalites, and silver halides are even less water-soluble than silver hydroxides.

In order to check the accuracy of our calculated DFT results given the unsuccessful ion exchange experiments, we compare our computational model with experimental findings of Mikuła et al. [53] for $|Pb_4Cl_2|$ -SOD, $|Cd_4Cl_2|$ -SOD, and $|Ag_8Cl_2|$ -SOD. Fig. 2 shows this comparison, along with the experimental infrared spectra and band assignments of natural sodalite as well as sodalite exchanged with Ag^+ , Cd^{2+} , and Pb^{2+} cations.

It is worth mentioning that silver exchange was complete in Mikuła et al.'s work [53], which resulted in a similar infrared spectrum compared to that of the parent $|Na_8Cl_2|$ -SOD. Qualitatively, our results are in better agreement with experimental spectra than were the Hartree–Fock calculations in Mikuła et al.'s study. However, there is no obvious "signature" of Pb²⁺ or Cd²⁺ exchange evident in these spectra.

Changing from monovalent Ag⁺ to divalent Cd²⁺, the shape of the infrared spectrum changes significantly. The peaks in the asymmetric stretching region split into high- and low-wavenumber bands compared to natural sodalite. In addition, the symmetric stretching and bending regions show additional peaks. The reason why the shape of the IR spectrum changes and additional peaks are present for the sodalites exchanged with divalent cations is that the unit cell distorts slightly from perfect cubic symmetry, and therefore some vibrations generate changes in the dipole moment that would be IR-invisible in a perfectly cubic cell. It should be noted that such distortions would not likely be visible in a macroscopic crystal.

The agreement between experiment and simulation for cadmium is not as strong as in the silver case because (i) cadmium is not easily ion-exchanged into sodalite and the resulting IR spectrum is very sensitive to the procedure by which the ion exchange takes place [55], and (ii) the resolution of the spectrometer might not have been high enough to be able to deconvolute the IR spectra. However, our theoretical spectrum for $|Cd_4Cl_2|$ -SOD is in qualitative agreement with the spectrum calculated by Mikuła et al. [53].

Finally, a similar spectrum to that in the cadmium case is seen with the infrared spectrum of $|Pb_4Cl_2|$ -SOD. However, lead in general is more easily exchanged into sodalite compared to cadmium [55,56].

3.3. Ion exchange of anion-free sodalite

This section will explore the sensitivity of theoretical vibrational spectroscopy to K^+ , Cd^{2+} , and Pb^{2+} ions in anhydrous, anion-free sodalite ($|Na_6|$ -SOD) for different possible cation combinations. As mentioned earlier, six out of eight cationic sites are filled in an anion-free sodalite cage by monovalent cations. Similarly, this is reduced to three sites for divalent cations, and so on.

In the first step in our approach, we assume that the three cations (Pb $^{2+}$, Cd $^{2+}$, K $^+$) have been partially exchanged with Na $^+$ ions simultaneously, such that five Na $^+$ ions are exchanged with K $^+$, Cd $^{2+}$, and Pb $^{2+}$, and only one sodium cation remains in the structure (|NaKCdPb|-SOD). We then compared the vibrational spectra of this compound with other sodalites containing only one type of cation (|Na₆|-, |K₆|-, |Cd₃|-, or |Pb₃|-SOD). The results from this step are shown in Fig. 3. In the infrared spectra of compound |NaKCdPb|-SOD, there is a band at approximately 860 cm $^{-1}$, which also is present in the spectrum of |Cd₃|-SOD at the same wavenumber. However, because of the presence of a band at about 881 cm $^{-1}$ in the |Pb₃|-SOD, one cannot be certain as to whether it is caused by the presence of cadmium or lead in an experiment. Nevertheless, we might (in principle) be able to conclude that the lower the wavenumber of a band around this vicinity, the more likely that it is caused by the presence of cadmium than lead.

In order to be confident in our assignment, we first consider only the effect of cadmium in the presence of sodium and potassium as background without lead being present. Fig. 4 shows this comparison. In a neutral anhydrous sodalite, the possible configurations in a single-unit-cell calculation with these three cations present are $|Na_3KCd|$ -SOD, |

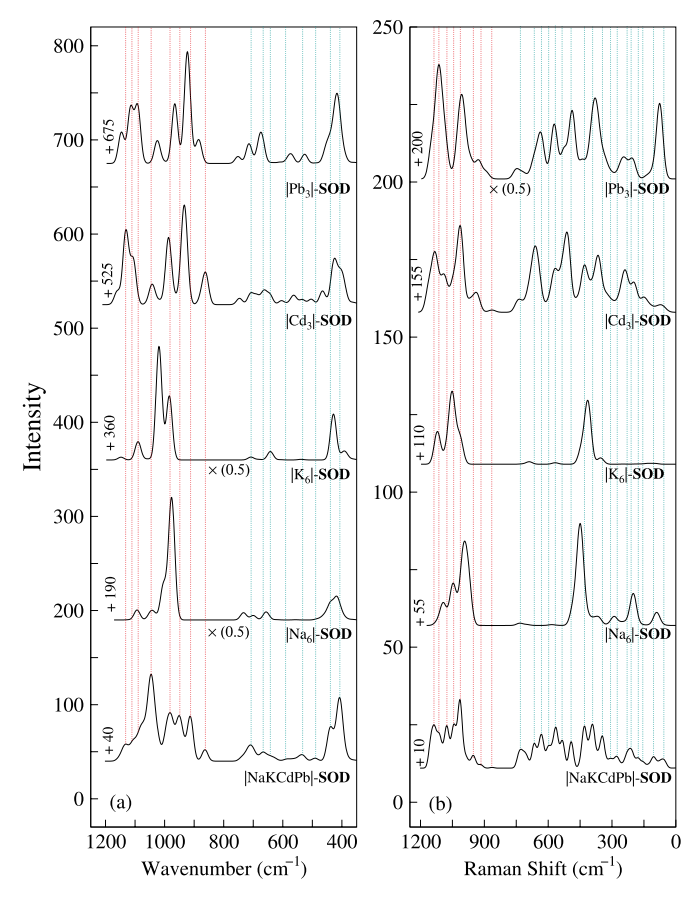


Fig. 3. Calculated (a) mid-infrared and (b) Raman spectra of anion-free sodalite exchanged with different cations. The bottom spectrum in each graph corresponds to sodalite containing all four cations (|NaKCdPb|-SOD). The intensity is proportional to absorbance and has units of C^2 m⁻⁴ Å⁻² amu⁻¹ in the case of infrared; in the case of Raman, it is proportional to scattering intensity with units of Å⁴ amu⁻¹. The values written below/above the graphs are the numbers by which they are scaled/translated. Dashed lines are to guide the eye starting from the bands in |NaKCdPb|-SOD. Red denotes the asymmetric stretching region and green denotes the symmetric stretching and bending modes. (For interpretation of the references to color in this figure legend, the reader is referred to the Web version of this article.)

 $Na_2K_2Cd|$ -SOD, and $|NaKCd_2|$ -SOD. These are the bottom three spectra in Fig. 4. As seen in Fig. 4, the band at approximately $860~cm^{-1}$ in both the infrared and Raman spectra of $|Cd_3|$ -SOD is also observable in the materials with all three cations present (bottom three graphs in Fig. 4). Another possible case that could occur for anhydrous anion-free sodalite in an ion exchange processes is that sodalite exchanges with potassium and lead but not cadmium. The possible configurations for this case are $|Na_3KPb|$ -SOD, $|Na_2K_2Pb|$ -SOD, and $|NaKPb_2|$ -SOD.

Fig. 5 also compares the infrared as well as Raman spectra of these three compounds with structures in which all cations are the same. The purpose of this comparison is to see whether lead is evident in the presence of background of sodium and potassium, which are ordinarily present in water resources. As shown in Fig. 5, there is a shoulder at around 883 cm $^{-1}$ in the infrared spectra as well as Raman spectra for all three partially-exchanged compositions that is present in $|Pb_3|$ -SOD but not $|Na_6|$ -SOD or $|K_6|$ -SOD. It should be noted that there is no distinct peak in the low wavenumber range (symmetric stretching and bending modes) for any of the situations that we have discussed so far that can be traced back to $|Na_6|$ -SOD, $|K_6|$ -SOD, or $|Pb_3|$ -SOD. Note that farinfrared (FIR) does not provide any particular information about cation exchange, which is why we have discussed only the mid-infrared (MIR) range.

As an example of sodalite partially exchanged with Cd²⁺ and Pb²⁺,

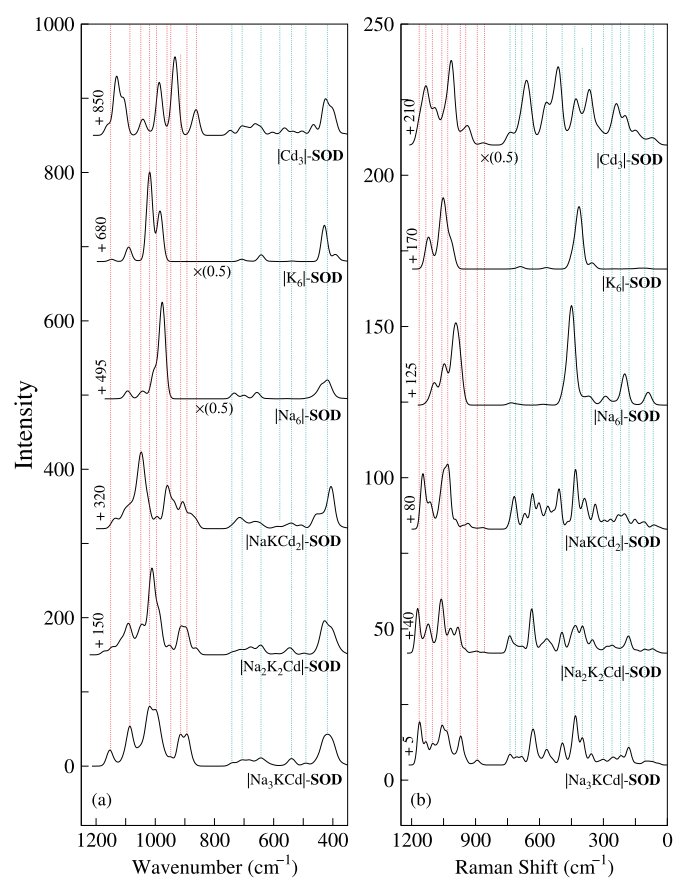


Fig. 4. Calculated (a) mid-infrared and (b) Raman spectra of anion-free sodalites partially-exchanged with different cations. The bottom spectrum in each graph corresponds to sodalite containing Na $^+$, K $^+$, and Cd $^{2+}$ cations. The intensity is proportional to absorbance and has units of C 2 m $^{-4}$ Å $^{-2}$ amu $^{-1}$ in the case of infrared; in the case of Raman, it is proportional to scattering intensity with units of Å 4 amu $^{-1}$. The values written below/above the graphs are the numbers by which they are scaled/translated. Dashed lines are to guide the eye starting from the bands in sodalites containing these three cations. Red denotes the asymmetric stretching region and green denotes the symmetric stretching and bending modes. (For interpretation of the references to color in this figure legend, the reader is referred to the Web version of this article.)

we chose to study $|Na_2CdPb|$ -SOD, which is the only possible way to create a single periodic unit cell with all three ions present. Fig. 6 compares the vibrational spectra of the aforementioned material with sodium-only, cadmium-only, and lead-only anhydrous sodalites. Similar to our previous reasoning, the presence of a band at approximately 870 cm $^{-1}$ in both infrared and Raman spectra is evidence of the presence of cadmium and/or lead in the structure. The key point here is that the presence of lead tends to shift this vibration to higher wavenumbers, up to 885 cm $^{-1}$, and cadmium red-shifts this band to 860 cm $^{-1}$.

Finally, in order to be convinced that this band only exists when either cadmium or lead is present in sodalite and is not caused by the presence of potassium, we compared the infrared and Raman spectra of sodalite when only potassium and sodium are exchanged. The results from this comparison are provided in Fig. S4 in the Supplementary Data. Throughout the ion exchange process with potassium, no band will appear within the $860-880~\text{cm}^{-1}$ region, which provides more evidence that the band in the $860-880~\text{cm}^{-1}$ range only occurs because of cadmium and/or lead. Nevertheless, one could argue that the aforementioned band might get masked by ions such as Mg^{2+} , Ca^{2+} , which are prevalent in water resources. In addition, we also have considered two other heavy metal cations, Ag^+ and Hg^{2+} . Fig. 7 shows that there is no band in the $860-880~\text{cm}^{-1}$ region for any of the compounds except for |

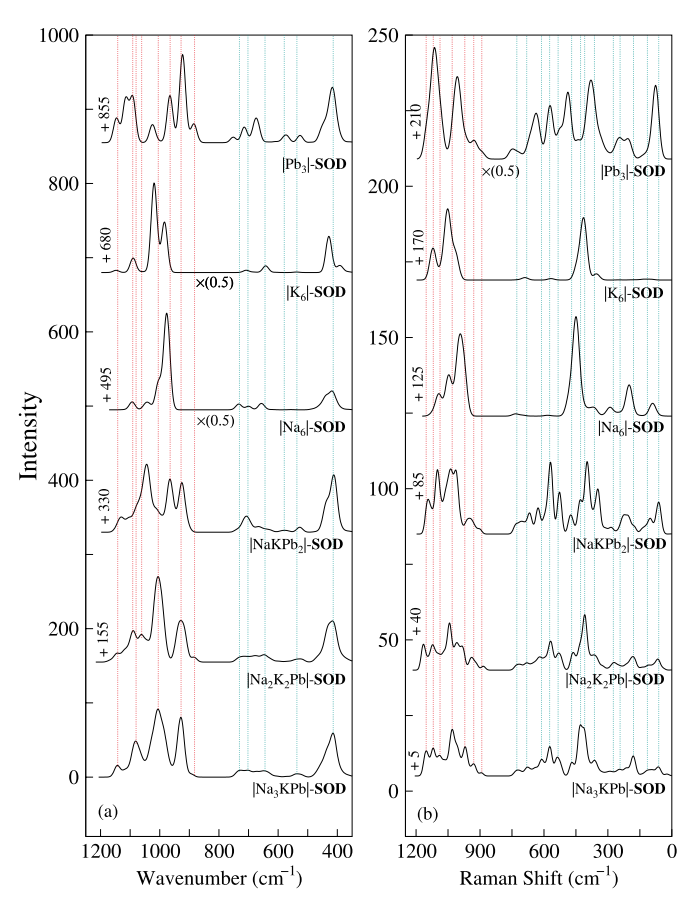


Fig. 5. Calculated (a) mid-infrared and (b) Raman spectra of anion-free sodalite exchanged with different cations. The bottom spectrum in each graph corresponds to sodalite containing Na $^+$, K $^+$, and Pb $^{2+}$ cations. The intensity is proportional to absorbance and has units of C^2 m $^{-4}$ Å $^{-2}$ amu $^{-1}$ in the case of infrared; in the case of Raman, it is proportional to scattering intensity with units of Å 4 amu $^{-1}$. The values written below/above the graphs are the numbers by which they are scaled/translated. Dashed lines are to guide the eye starting from the bands in sodalites containing these three cations. Red denotes the asymmetric stretching region and green denotes the symmetric stretching and bending modes. (For interpretation of the references to color in this figure legend, the reader is referred to the Web version of this article.)

 $Hg_3|$ -SOD, which has a shoulder at approximately 855 cm $^{-1}$. This observation suggests that the appearance of a band in the vicinity of 860–880 cm $^{-1}$ in the spectra of anion-free sodalite may indicate the presence of cadmium, lead, and/or mercury. However, the relatively low intensity of this shoulder means it will be difficult to distinguish from background and/or line-broadening effects in experimental infrared spectra.

3.4. Infrared and Raman signatures of hydroxysodalite

So far, based on DFT calculations, we have observed the effects of extra-framework cations on the infrared and Raman spectra of sodalite both individually and when accompanied by other cations. Most of the peaks that are seen in a partially-exchanged hypothetical sodalite structure (i.e., sodalite that contains different extra-framework species) are similar to peaks found in the spectra of sodalites that contain only one type of extra-framework cation. In other words, if there is no overlap of bands in the spectra of sodalite containing one extra-framework species, those peaks will still appear even when other cations are present.

Following this observation, let us examine the sensitivity of the theoretical vibrational spectra of anhydrous hydroxysodalite, |

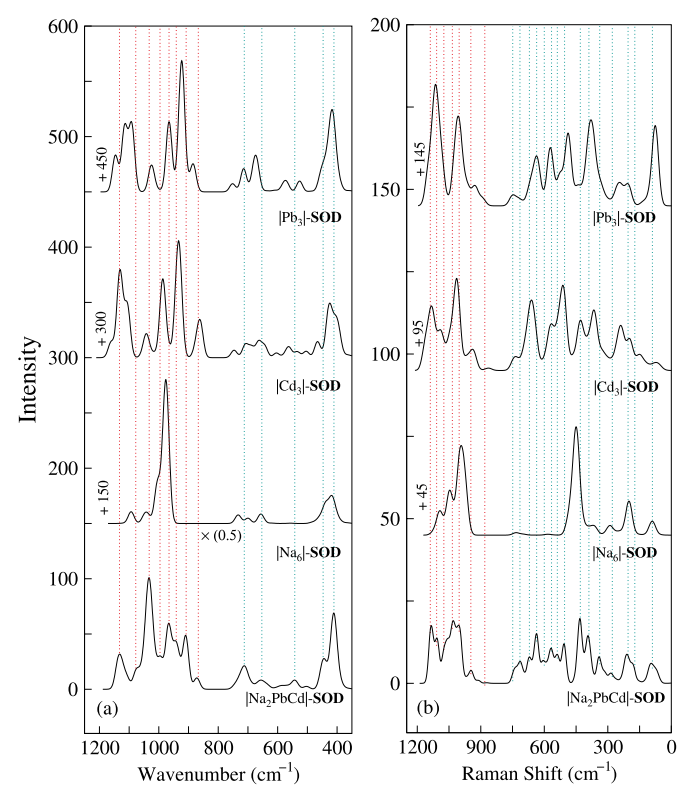


Fig. 6. Calculated (a) mid-infrared and (b) Raman spectra of anion-free sodalite exchanged with different cations. The bottom spectrum in each graph corresponds to sodalite containing Na $^+$, Cd $^{2+}$, and Pb $^{2+}$ cations. The intensity is proportional to absorbance and has units of $G^2 m^{-4} \mathring{A}^{-2} amu^{-1}$ in the case of infrared; in the case of Raman, it is proportional to scattering intensity with units of \mathring{A}^4 amu $^{-1}$. The values written below/above the graphs are the numbers by which they are scaled/translated. Dashed lines are to guide the eyes starting from the bands in sodalites containing these three cations. Red denotes the asymmetric stretching region and green denotes the symmetric stretching and bending modes. (For interpretation of the references to color in this figure legend, the reader is referred to the Web version of this article.)

 $Na_8(OH)_2|$ -**SOD**, after Pb^{2+} , Hg^{2+} , Cd^{2+} , K^+ , Mg^{2+} , and Ca^{2+} exchange. The choice of hydroxysodalite over other anion-bearing sodalites, such as bromosodalites, was inspired by Golbad et al. [56], who examined the capacity of hydroxysodalite for the removal of lead. They estimated that sodalite's cation exchange capacity is 98.1% for a solution of 100 mg/L of lead nitrate at a pH of 6 at room temperature. Equilibrium was reached after 6 h. Lack of infrared and/or Raman spectral evidence from the aforementioned investigation encouraged us to study the sensitivity of vibrational spectroscopy of hydroxysodalite with respect not only to lead but also to other extra-framework species.

Figs. 8 and 9 show the mid- and high-frequency ranges, respectively, of both the infrared and Raman spectra of anhydrous hydroxysodalite for different extra-framework cations. In contrast to anion-free sodalites, $|{\rm Pb_4(OH)_2}\>|\text{-SOD}\>$, $|{\rm Ca_4(OH)_2}\>|\text{-SOD}\>$, $|{\rm K_8(OH)_2}\>|\text{-SOD}\>$, and $|{\rm Na_8(OH)_2}\>|\text{-SOD}\>$ do not exhibit any bands in the 850–880 cm $^{-1}$ range. However, for the ${\rm Mg^{2+}}$, ${\rm Cd^{2+}}$, and ${\rm Hg^{2+}}$ cases, there are some bands and/or shoulders either inside or in the vicinity of this range. Therefore, relying solely on the 850–880 cm $^{-1}$ range is not an infallible indicator for the presence of heavy metals in sodalites because (i) lead-exchanged hydroxy-, chloro-, or bromo-sodalites do not have bands in this range to begin with, and (ii) magnesium-exchanged hydroxysodalite has a band which might mask the presence of heavy metals.

On the other hand, because of the presence of hydroxide anion (OH $^-$), the high-frequency range for the OH stretching mode should be taken into account along with the 850–880 cm $^{-1}$ range. Fig. 9 shows the high-frequency range of hydroxysodalite exchanged with the Na $^+$,

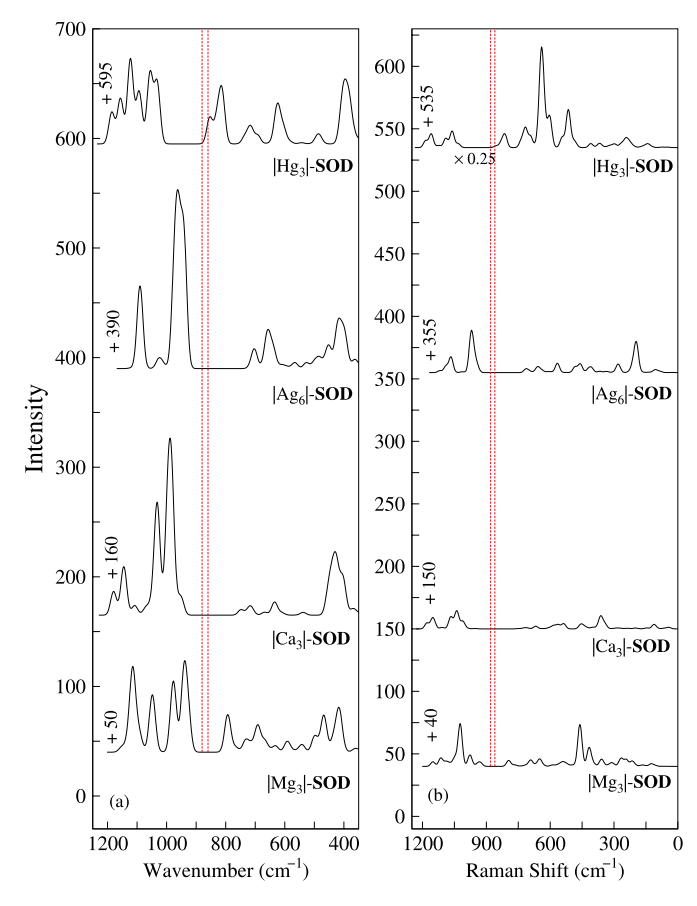


Fig. 7. Calculated (a) mid-infrared and (b) Raman spectra of anion-free sodalite exchanged with different cations. The intensity is proportional to absorbance and has units of $C^2 \, m^{-4} \, \mathring{A}^{-2} \, amu^{-1}$ in the case of infrared; in the case of Raman, it is proportional to scattering intensity with units of $\mathring{A}^4 \, amu^{-1}$. The values written below/above the graphs are the numbers by which they are scaled/translated. Dashed lines are to guide the eye to the see the differences between compounds between 860 and 880 cm⁻¹.

 ${\rm Mg}^{2+}, {\rm K}^+, {\rm Ca}^{2+}, {\rm Cd}^{2+}, {\rm Hg}^{2+},$ and ${\rm Pb}^{2+}$ cations. The first thing to note is that OH stretching is not IR-active in some cases, such as |Na₈(OH)₂|-SOD and |K₈(OH)₂|-SOD. As seen in Fig. 9, lead- and mercuryexchanged sodalite exhibit OH stretching bands within 30 cm⁻¹ of each other. However, these vibrational modes for the |Cd₄(OH)₂|-**SOD** and $|Mg_4(OH)_2|$ -SOD occur at virtually the same wavenumber (\approx 3631-3633 cm⁻¹), which suggests that differentiating them would be difficult. The only possible way to distinguish magnesium-exchanged sodalites from cadmium-exchanged sodalites would be to compare their Raman spectra in the vicinity of 560 cm⁻¹, as in Fig. 8. In these spectra, there is a sharp peak for the magnesium-exchanged sodalite, whereas cadmium-exchanged sodalite does not exhibit this peak. Though it has been shown [57–59] that OH stretching vibrations can be detected for IR and Raman spectra in systems such as hemimorphite, water clusters, and sucrose crystals, such detection in zeolites would be challenging: the weak nature of Raman scattering combined with the strong fluorescence of zeolites often results in Raman spectra with high background levels [31].

3.5. Possible applications and further investigations

Our target application of this line of study was to detect lead, cadmium, or mercury in ground water. However, our investigation of anion-bearing sodalites has revealed that, though the $850-880~{\rm cm}^{-1}$ range could conceivably provide a signature of mercury, lead, or cadmium in anion-free zeolites, such a signal would be weak and could be masked by

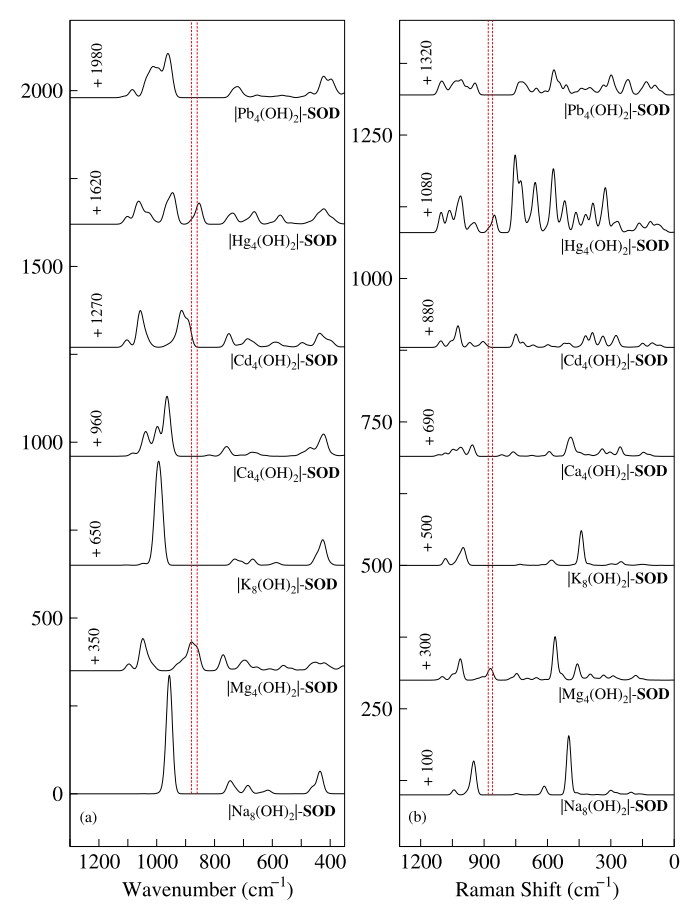


Fig. 8. Calculated (a) mid-infrared infrared and (b) Raman spectra of anhydrous hydroxysodalite, $Na_8(OH)_2$ -**SOD** as a function of different cations. The intensity is proportional to absorbance and has units of C^2 m⁻⁴ Å⁻² amu⁻¹ in the case of infrared; in the case of Raman, it is proportional to scattering intensity with units of Å⁴ amu⁻¹. The values written next to the graphs are the numbers by which they are translated. Dashed lines are to guide the eye to the see the differences between compounds between 860 and 880 cm⁻¹.

magnesium hydroxysodalites.

To be useful as a detector, the loading of heavy metal cations on the zeolite would have to be high enough to see differences in the IR spectrum at ion concentrations at or below the relevant safety thresholds established by regulatory agencies. The lowest acceptable concentrations of lead, cadmium, and mercury in drinking water based on Environmental Protection Agency regulations [60] are 15, 5, and 2 ppb (μg/kg), respectively. According to Somerset et al. [61,62], zeolites synthesized using coal fly ash are able to reduce lead concentrations from 1.50 to 0.25 ppb, cadmium concentrations from 0.80 to 0.45 ppb, and mercury concentrations from 0.47 ppb to 0.17 ppb. In addition, a similar study by Golbad et al. [56] showed that a loading (based on the Langmuir isotherm) of one Pb²⁺ cation per sodalite cage corresponds to a solution with a concentration as high as 2 ppm. This is significantly higher than the threshold imposed by the EPA (15 ppb). Therefore, we anticipate the intensity of the band in the 850–880 cm⁻¹ range might not be high enough to detect concentrations on the order of parts per billion. However, to the best of our knowledge, there is not a study in which this question has been addressed experimentally.

In any case, a relatively sensitive spectrometer would be required to distinguish the weak shoulder that results from lead, cadmium, or mercury exchange of anion-free sodalites, even at full saturation. Fortunately, with the advancement of technology in the spectroscopy realm, there exist infrared and Raman spectrometers that have resolutions as high as 0.04 cm^{-1} [63], which is likely to be sensitive enough to

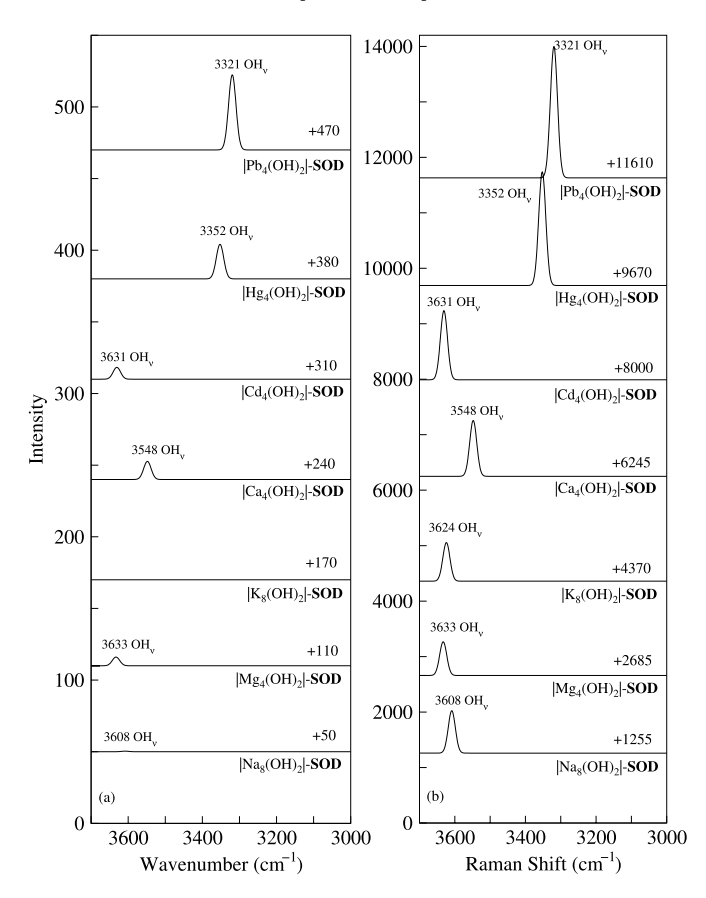


Fig. 9. Calculated (a) infrared and (b) Raman spectra of anhydrous hydroxysodalite, $Na_8(OH)_2$ -**SOD** as a function of different cations at higher frequencies. OH_ν represents the stretching mode, and the intensity is proportional to absorbance and has units of $C^2 \, m^{-4} \, \mathring{A}^{-2} \, amu^{-1}$ in the case of infrared and $\mathring{A}^4 \, amu^{-1}$ for Raman. The values written above the graphs are the numbers by which they are translated.

resolve the bands in the 850–880 cm⁻¹ range. However, more work is required to ascertain whether the infrared and Raman spectra of exchanged hydroxysodalites may enable even the qualitative detection of the heavy metals lead, cadmium, and mercury for concentrations as low as 2 ppb. At this stage, we do not anticipate IR detection of heavy metals to be sensitive enough for water resource management, primarily because the intensity of the relevant IR signals is not high enough.

4. Conclusions

We have examined the sensitivity of theoretical infrared and Raman spectra of sodalites to Mg^{2+} , K^+ , Ca^{2+} , Ag^+ , Cd^{2+} , Pb^{2+} , and Hg^{2+} ion exchange. This was done to investigate whether there exists a "signature" indicating the presence of heavy metals, even when other ions (such as potassium, magnesium, and calcium) that are normally present in ground water are present in the background. Our results suggest that the presence of bands in the 850–880 cm $^{-1}$ range in either the IR or Raman spectra can be attributed to the presence of cadmium, lead, or mercury in anion-free sodalites. Our density functional theory (DFT) predictions are in good agreement with previously published studies [53,55]. However, the intensities of these features are likely not high enough to use them as indicators of cadmium, lead, or mercury contamination.

We anticipate that the calculated infrared and Raman spectra of ion-exchanged sodalites presented here will be useful in future experimental characterization of ion-exchanged zeolites, regardless of the final application.

Declaration of competing interest

The authors declare that they have no known competing financial interests or personal relationships that could have appeared to influence the work reported in this paper.

CRediT authorship contribution statement

Amir Mehdi Mofrad: Conceptualization, Data curation, Formal analysis, Investigation, Methodology, Validation, Visualization, Writing - original draft, Writing - review & editing. Parker S. Schellenberg: Data curation, Investigation, Methodology, Writing - original draft. Caio Peixoto: Investigation, Methodology, Heather K. Hunt: Funding acquisition, Project administration, Resources, Supervision, Writing - review & editing. Karl D. Hammond: Conceptualization, Funding acquisition, Project administration, Resources, Supervision, Visualization, Writing - review & editing.

Acknowledgments

Partial financial support for this work was provided by the National Science Foundation under award number DMR-1757936. Additional support was provided by the University of Missouri Research Board under award RB16-30. The computations in this work were performed on the high-performance computing infrastructure provided in part by Research Computing Support Services at the University of Missouri and in part by the National Science Foundation under grant number CNS-1429294.

Appendix A. Supplementary data

Supplementary data to this article can be found online at https://doi.org/10.1016/j.micromeso.2019.109983.

References

- L. Joseph, B.-M. Jun, J.R. Flora, C.M. Park, Y. Yoon, Removal of heavy metals from water sources in the developing world using low-cost materials: a review, Chemosphere 229 (2019) 142–159, https://doi.org/10.1016/j. chemosphere.2019.04.198.
- [2] L.M. Saran, T.C.T. Pissarra, G.A. Silveira, M.T.L. Constancio, W.J. de Melo, L.M. C. Alves, Land use impact on potentially toxic metals concentration on surface water and resistant microorganisms in watersheds, Ecotoxicol. Environ. Saf. 166 (2018) 366–374, https://doi.org/10.1016/j.ecoenv.2018.09.093.
- [3] R. Ghosh, A. Sahu, S. Pushpavanam, Removal of trace hexavalent chromium from aqueous solutions by ion foam fractionation, J. Hazard Mater. 367 (2019) 589–598, https://doi.org/10.1016/j.jhazmat.2018.12.105.
- [4] Y. Li, P. Bai, Y. Yan, W. Yan, W. Shi, R. Xu, Removal of Zn²⁺, Pb²⁺, Cd²⁺, and Cu²⁺ from aqueous solution by synthetic clinoptilolite, Microporous Mesoporous Mater. 273 (2019) 203–211, https://doi.org/10.1016/j.micromeso.2018.07.010.
- [5] F. Liu, W. Xiong, X. Feng, L. Shi, D. Chen, Y. Zhang, A novel monolith ZnS-ZIF-8 adsorption material for ultra effective Hg (II) capture from wastewater, J. Hazard Mater. 367 (2019) 381–389, https://doi.org/10.1016/j.jhazmat.2018.12.098.
- [6] G. Chen, Electrochemical technologies in wastewater treatment, Separ. Purif. Technol. 38 (1) (2004) 11–41, https://doi.org/10.1016/j.seppur.2003.10.006.
- [7] L. Charerntanyarak, Heavy metals removal by chemical coagulation and precipitation, Water Sci. Technol. 39 (10–11) (1999) 135–138, https://doi.org/ 10.1016/S0273-1223(99)00304-2.
- [8] A. Dąbrowski, Z. Hubicki, P. Podkoscielny, E. Robens, Selective removal of the heavy metal ions from waters and industrial wastewaters by ion-exchange method, Chemosphere 56 (2004) 91–106, https://doi.org/10.1016/j. chemosphere.2004.03.006.
- [9] O.F. González Vázquez, M.R. Moreno Virgen, V. Hernández Montoya, R. Tovar Gómez, J.L. Alcántara Flores, M.A. Pérez Cruz, M.A. Montes Morán, Adsorption of heavy metals in the presence of a magnetic field on adsorbents with different magnetic properties, Ind. Eng. Chem. Res. 55 (34) (2016) 9323–9331, https://doi. org/10.1021/acs.iecr.6b01990.
- [10] G.B. Dirisu, U.C. Okonkwo, I.P. Okokpujie, O.S. Fayomi, Comparative analysis of the effectiveness of reverse osmosis and ultraviolet radiation of water treatment, J. Ecol. Eng. 20 (1) (2019) 61–75, https://doi.org/10.12911/22998993/93978.
- [11] F. Fu, Q. Wang, Removal of heavy metal ions from wastewaters: a review, J. Environ. Manag. 92 (3) (2011) 407–418, https://doi.org/10.1016/j. jenvman.2010.11.011.

- [12] M. Zhao, Y. Xu, C. Zhang, H. Rong, G. Zeng, New trends in removing heavy metals from wastewater, Appl. Microbiol. Biotechnol. 100 (15) (2016) 6509–6518, https://doi.org/10.1007/s00253-016-7646-x.
- [13] S.M. Auerbach, K.A. Carrado, P.K. Dutta, Handbook of Zeolite Science and Technology, Marcel Dekker, New York, 2003.
- [14] J. Čejka, H. van Bekkum, A. Corma, F. Schüth, Introduction to zeolite science and practice, in: third ed.Stud. Surf. Sci. Catal, 168, Elsevier, Amsterdam, 2007.
- [15] W. Loewenstein, The distribution of aluminum in the tetrahedra of silicates and aluminates, Am. Mineral. 39 (1–2) (1954) 92–96.
- [16] C. Baerlocher, L.B. McCusker, Database of zeolite structures. http://www.iza-structure.org/databases/.
- [17] W.H. Baur, R.X. Fischer, A historical note on the sodalite framework: the contribution of Frans Maurits Jaeger, Microporous Mesoporous Mater. 116 (1–3) (2008) 1–3, https://doi.org/10.1016/j.micromeso.2008.04.005.
- [18] G.A. Ozin, A. Kuperman, A. Stein, Advanced zeolite materials science, Angew. Chem. Int. Ed. 28 (3) (1989) 359–376, https://doi.org/10.1002/anie.198903591.
- [19] P. Aprea, D. Caputo, N. Gargiulo, B. de Gennaro, F. Iucolano, B. Liguori, C. Colella, Ion exchange kinetics and thermodynamics of hydrosodalite, a narrow pore zeolite, J. Porous Mater. 21 (5) (2014) 643–651, https://doi.org/10.1007/s10934-014-9810-v.
- [20] A. Hassib, O. Beckman, H. Annersten, Photochromic properties of natural sodalite, J. Phys. D Appl. Phys. 10 (5) (1977) 771–777, https://doi.org/10.1088/0022-3727/10/5/018
- [21] A. Stein, G.A. Ozin, P.M. Macdonald, G.D. Stucky, R. Jelinek, Silver, sodium halosodalites: class A sodalites, J. Am. Chem. Soc. 114 (13) (1992) 5171–5186, https://doi.org/10.1021/ja00039a032.
- [22] G.V. Shanbhag, M. Choi, J. Kim, R. Ryoo, Mesoporous sodalite: a novel, stable solid catalyst for base-catalyzed organic transformations, J. Catal. 264 (1) (2009) 88–92, https://doi.org/10.1016/j.jcat.2009.03.014.
- [23] S. Bordiga, C. Lamberti, F. Bonino, A. Travert, F. Thibault-Starzyk, Probing zeolites by vibrational spectroscopies, Chem. Soc. Rev. 44 (20) (2015) 7262–7341, https://doi.org/10.1039/C5CS00396B.
- [24] Y. Ma, Z. Liu, A. Geng, T. Vogt, Y. Lee, Structural and spectroscopic studies of alkali-metal exchanged stilbites, Microporous Mesoporous Mater. 224 (2016) 339–348, https://doi.org/10.1016/j.micromeso.2016.01.005.
- [25] M. Łodziński, R. Wrzalik, M. Sitarz, Micro-Raman spectroscopy studies of some accessory minerals from pegmatites of the Sowie Mts and Strzegom-Sobótka massif, Lower Silesia, Poland, J. Mol. Struct. 744–747 (2005) 1017–1026, https:// doi.org/10.1016/i.molstruc.2004.12.015.
- [26] Flanigen E. M., Khatami H., Szymanski H. A., Infrared structural studies of zeolite frameworks, in: Flanigen E. M., Sand L. B. (Eds.), Molecular Sieve Zeolites-I, Adv. Chem., American Chemical Society, Washington, DC, August 1, 1974, Ch. 16, pp. 201–229. doi:10.1021/ba-1971-0101.ch016.
- [27] P. Makreski, G. Jovanovski, B. Kaitner, Minerals from Macedonia. XXIV. Spectrastructure characterization of tectosilicates, J. Mol. Struct. 924–926 (2009) 413–419, https://doi.org/10.1016/j.molstruc.2009.01.001.
- [28] V. Van Speybroeck, K. Hemelsoet, L. Joos, M. Waroquier, R.G. Bell, C.R.A. Catlow, Advances in theory and their application within the field of zeolite chemistry, Chem. Soc. Rev. 44 (2015) 7044–7111, https://doi.org/10.1039/C5CS00029G.
- [29] A.M. Mofrad, C. Peixoto, J. Blumeyer, J. Liu, H.K. Hunt, K.D. Hammond, Vibrational spectroscopy of sodalite: theory and experiments, J. Phys. Chem. 122 (43) (2018) 24765–24779, https://doi.org/10.1021/acs.jpcc.8b07633.
- [30] M. Król, W. Mozgawa, W. Jastrzębski, Theoretical and experimental study of ion-exchange process on zeolites from 5-1 structural group, J. Porous Mater. 23 (1) (2016) 1–9, https://doi.org/10.1007/s10934-015-0050-6.
- [31] K.D. Hammond, M. Gharibeh, G.A. Tompsett, F. Dogan, A.V. Brown, C.P. Grey, S. M. Auerbach, Wm C. Conner Jr., Optimizing the synthesis of nitrogen substituted zeolites, Chem. Mater. 22 (1) (2010) 130–142, https://doi.org/10.1021/cm902511a.
- [32] A. Mikula, M. Król, A. Koleżyński, The influence of the long-range order on the vibrational spectra of structures based on sodalite cage, Spectrochim. Acta A Mol. Biomol. Spectros. 144 (2015) 273–280, https://doi.org/10.1016/j. saa.2015.02.073.
- [33] E.C. Moloy, R.T. Cygan, F. Bonhomme, D.M. Teter, A. Navrotsky, Molecular simulations of anhydrous $Na_6[Al_6Si_6O_{24}]$ sodalite, Chem. Mater. 16 (11) (2004) 2121–2133, https://doi.org/10.1021/cm0352302.
- [34] L. McCusker, F. Liebau, G. Engelhardt, Nomenclature of structural and compositional characteristics of ordered microporous and mesoporous materials with inorganic hosts: (IUPAC recommendations 2001), Microporous Mesoporous Mater. 58 (1) (2003) 3–13, https://doi.org/10.1016/S1387-1811(02)00545-0.
- [35] J. Felsche, S. Luger, C. Baerlocher, Crystal structures of the hydro-sodalite $Na_6[AlSiO_4]_6$ $8H_2O$ and of the anhydrous sodalite $Na_6[AlSiO_4]_6$, Zeolites 6 (5) (1986) 367-372, https://doi.org/10.1016/0144-2449(86)90064-3.
- [36] I. Hassan, H.D. Grundy, The crystal structures of sodalite-group minerals, Acta Crystallogr. B 40 (1984) 6–13, https://doi.org/10.1107/S0108768184001683.
- [37] P. Hohenberg, W. Kohn, Inhomogeneous electron gas, Phys. Rev. 136 (3B) (1964) B864–B871, https://doi.org/10.1103/PhysRev.136.B864.
- [38] W. Kohn, L.J. Sham, Self-consistent equations including exchange and correlation effects, Phys. Rev. 140 (4A) (1965) A1133–A1138, https://doi.org/10.1103/ PhysRev.140.A1133.
- [39] N. Troullier, J.L. Martins, Efficient pseudopotentials for plane-wave calculations, Phys. Rev. B 43 (3) (1991) 1993–2006, https://doi.org/10.1103/ PhysRevB.43.1993.
- [40] J.P. Perdew, Y. Wang, Accurate and simple analytic representation of the electrongas correlation energy, Phys. Rev. B 45 (23) (1992) 13244–13249, https://doi.org/ 10.1103/PhysRevB.45.13244.

- [41] L.H. Thomas, The calculation of atomic fields, Proc. Camb. Philos. Soc. 23 (1927) 542–548, https://doi.org/10.1017/S0305004100011683.
- [42] E. Fermi, Eine statistische methode zur bestimmung einiger eigenschaften des atoms und ihre anwendung auf die theorie des periodischen systems der elemente, Z. Phys. 48 (1–2) (1928) 73–79, https://doi.org/10.1007/BF01351576.
- [43] P.A.M. Dirac, Note on exchange phenomena in the Thomas atom, Proc. Camb. Philos. Soc. 26 (3) (1930) 376–385, https://doi.org/10.1017/ S0305004100016108.
- [44] S.H. Vosko, L. Wilk, M. Nusair, Accurate spin-dependent electron liquid correlation energies for local spin-density calculations—A critical analysis, Can. J. Phys. 58 (8) (1980) 1200–1211, https://doi.org/10.1139/p80-159.
- [45] P. Giannozzi, S. Baroni, N. Bonini, M. Calandra, R. Car, C. Cavazzoni, D. Ceresoli, G.L. Chiarotti, M. Cococcioni, I. Dabo, A. Dal Corso, S. de Gironcoli, S. Fabris, G. Fratesi, R. Gebauer, U. Gerstmann, C. Gougoussis, A. Kokalj, M. Lazzeri, L. Martin-Samos, N. Marzari, F. Mauri, R. Mazzarello, S. Paolini, A. Pasquarello, L. Paulatto, C. Sbraccia, S. Scandolo, G. Sclauzero, A.P. Seitsonen, A. Smogunov, P. Umari, R.M. Wentzcovitch, QUANTUM ESPRESSO: A modular and open-source software project for quantum simulations of materials, J. Phys. Condens. Matter 21 (39) (2009) 395502_495522, https://doi.org/10.1088/0953-8984/21/39/395502. http://www.quantum-espresso.org.
- [46] H.J. Monkhorst, J.D. Pack, Special points for Brillouin-zone integrations, Phys. Rev. B 13 (12) (1976) 5188–5192, https://doi.org/10.1103/PhysRevB.13.5188.
- [47] P. Hennig, M. Kiefel, Quasi-Newton methods: a new direction, J. Mach. Learn. Res. 14 (2013) 843–865.
- [48] R.M. Pick, M.H. Cohen, R.M. Martin, Microscopic theory of force constants in the adiabatic approximation, Phys. Rev. B 1 (2) (1970) 910–920, https://doi.org/ 10.1103/PhysRevB.1.910.
- [49] G. Placzek, Rayleigh–Streuung und Raman-effekt, in: E. Marx (Ed.), Handbuch Der Radiologie, vol. I, Akademische Verlagsgesellschaft, Leipzig, 1934, pp. 205–374.
- [50] R.D. Shannon, Revised effective ionic radii and systematic studies of interatomic distances in halides and chalcogenides, Acta Crystallogr. A 32 (1976) 751–767, https://doi.org/10.1107/S0567739476001551.
- [51] M. Brik, I. Kityk, Modeling of lattice constant and their relations with ionic radii and electronegativity of constituting ions of AXY cubic crystals (A=K, Cs, Rb, Tl; X=tetravalent cation, Y=F, Cl, Br, I), J. Phys. Chem. Solids 72 (11) (2011) 1256–1270, https://doi.org/10.1016/j.jpcs.2011.07.016.

- [52] S.E. Latturner, J. Sachleben, B.B. Iversen, J. Hanson, G.D. Stucky, Covalent guest–framework interactions in heavy metal sodalites: structure and properties of thallium and silver sodalite, J. Phys. Chem. B 103 (34) (1999) 7135–7144, https:// doi.org/10.1021/jp990898i.
- [53] A. Mikuła, M. Król, A. Koleżyński, Experimental and theoretical spectroscopic studies of Ag-, Cd- and Pb-sodalite, J. Mol. Struct. 1126 (2016) 110–116, https:// doi.org/10.1016/j.molstruc.2016.03.004.
- [54] H. Lechert, The pH-value and its importance for the crystallization of zeolites, in: H. Robson, K.P. Lillerud (Eds.), Verified Syntheses of Zeolitic Materials, Elsevier Science, Amsterdam, 2001, pp. 33–38. Ch. 5.
- [55] S. Eiden-Assmann, New heavy metal-hydro-sodalites containing Cd²⁺, Ag⁺ or Pb²⁺: synthesis by ion-exchange and characterisation, Mater. Res. Bull. 37 (5) (2002) 875–889, https://doi.org/10.1016/S0025-5408(02)00715-8.
- [56] S. Golbad, P. Khoshnoud, N. Abu-Zahra, Hydrothermal synthesis of hydroxy sodalite from fly ash for the removal of lead ions from water, Int. J. Environ. Sci. Technol. 14 (1) (2017) 135–142, https://doi.org/10.1007/s13762-016-1133-x.
- [57] B. Kolesov, Raman investigation of H₂O molecule and hydroxyl groups in the channels of hemimorphite, Am. Mineral. 91 (8–9) (2006) 1355–1362.
- [58] Q. Sun, The Raman OH stretching bands of liquid water, Vib. Spectrosc. 51 (2) (2009) 213–217, https://doi.org/10.1016/j.vibspec.2009.05.002.
- [59] J. Giermańska, M.M. Szostak, Polarized Raman and infrared spectra of OH stretching vibrations in the sucrose crystal, J. Raman Spectrosc. 22 (2) (1991) 107–109, https://doi.org/10.1002/jrs.1250220211.
- [60] National Primary Drinking Water Regulations, Tech. Rep. 816-F-09-004, U. S. Environmental Protection Agency, May 2009. https://www.epa.gov/sites/pr oduction/files/2016-06/documents/npwdr complete table.pdf.
- [61] V. Somerset, L. Petrik, E. Iwuoha, Alkaline hydrothermal conversion of fly ash filtrates into zeolites 2: utilization in wastewater treatment, J. Environ. Sci. Health A 40 (8) (2005) 1627–1636, https://doi.org/10.1081/ESE-200060675.
- [62] V. Somerset, L. Petrik, E. Iwuoha, Alkaline hydrothermal conversion of fly ash precipitates into zeolites 3: the removal of mercury and lead ions from wastewater, J. Environ. Manag. 87 (1) (2008) 125–131, https://doi.org/10.1016/j. jenyman.2007.01.033.
- [63] A. Baraldi, P. Bertoli, R. Capelletti, A. Ruffini, A. Scacco, High-resolution vibrational spectroscopy of Pb-OH defects in KMgF₃ fluoroperovskite single crystals, Phys. Rev. B 63 (13) (2001) 134302, https://doi.org/10.1103/ PhysRevB.63.134302.